# Random cuts in binary mixtures of spheres

Annie Gervois
*Service de Physique Théorique, DSM, CEA/Saclay, F-91191 Gif-sur-Yvette Cedex, France*

Luc Oger* and Jean-Paul Troadec†
*Groupe Matière Condensée et Matériaux, UMR CNRS 6626, Université de Rennes I, F-35042 Rennes Cedex, France*
(Received 8 January 2004; published 29 September 2004)

Three-dimensional (3D) disordered media may be studied by performing random planar cuts through the material and trying to go back to 3D geometry from two-dimensional information. We have studied from this point of view numerical packings of spheres of two sizes for which the radii of the spheres and the composition of the mixtures have been obtained from the cuts. We have also studied the froths generated by the related Laguerre–Voronoi tessellation of the packings, and their cuts. Stereological relations, in this specific frame, are derived in both cases.

DOI: 10.1103/PhysRevE.70.031112 PACS number(s): 46.65.+g, 83.80.Fg, 61.43.Bn, 02.40.Pc

## I. INTRODUCTION

Disordered three-dimensional (3D) systems are difficult to handle and—except in very special cases—it is very difficult to perform a precise analysis. A possible approach consists in performing two-dimensional (2D) random (stereological) cuts [1] through the material in order to get statistical informations on the 3D system from the 2D statistics. Some classical stereological relations exist such as volume, area, number per unit volume or area between 3D and 2D structures.

Two peculiar classes of materials are often considered for which more can be done because of the relative "simplicity" of the shapes involved. First, *unconsolidated granular materials*—at least when they are modeled by spherical hard nonoverlapping grains; cuts are disordered assemblies of unequal disks which distribution is known. Second, *froths* (or foams) e.g., biological cells, geological layers, soap assemblies,… where the full space may be considered as filled with polyhedral convex cells; cuts fill the plane by convex polygonal cells which metric and topological features may be studied easily.

Already some practical studies were done to correlate 2D informations to 3D structures:

(1) One can also notice the experimental study by Sanders [2] on natural opals. The samples consist in silica spheres of two sizes (0.36 and 0.21 $\mu$m diamater) and they present side by side ordered and disordered zones which differ by the composition and the packing fraction, as shown by electron microscopy of fracture surfaces (the fractures pass through the spheres and so exhibit planar sections of the spheres).

(2) Sonneville *et al.* [3] have obtained a biliquid foam by extraction of the continuous phase of an oil-in-water emulsion through centrifugation; observation of the foam by freeze fracture electron microscopy shows that the oil droplets have deformed into polyhedral cells.

As shown by that latter experiment, the studies of grain assemblies and foams are not too far from each other. To combine the two approaches, at least in numerical packings of spheres, it is also possible to generate a froth from a packing by performing the Voronoi (resp. Laguerre, or radical) tessellation [4] of the space in the monodisperse (resp. polydisperse) case, most geometrical features of the grains being analyzed together with the corresponding ones for the related tessellation. The main difference between a natural froth and a froth obtained by tessellation of a sphere packing is due to steric exclusion: The smallest cell for a disk assembly is the smallest grain of the packing. Such a study was done in the monodisperse case [5] with numerical packings of spheres—the only parameter being the packing fraction. Besides checking the validity of global conservation laws, it was possible to compare the polydisperse 2D system of section disks to an ordinary random disk assembly with the same packing fraction and the same size distribution. Both behave very closely. Moreover, as the section disk distribution is naturally peaked in a small range of values, the radical tessellation of the two assemblies verifies most statistical properties of monodisperse random disk assemblies, both on the topological and the metric levels.

But even if the structure of two-size mixtures of spheres has also been studied, mostly on packings built numerically (for example [6]), the detailed analysis of the correlation between 3D information and 2D measurements is not yet done completely. A lot of new tools, such as x-ray tomography, MRI, and confocal microscope, can deliver some kinds of 3D descriptions which can be analyzed also as a set of consecutive 2D dimensional slices. To get some informations from 2D images is not so easy without any a priori information, as we can see in the comparison between the real packing and one 2D cut in Fig. 1.

The aim of this paper is to begin an analysis for two-size mixtures of spheres generated numerically, similar to the one for monodisperse packings [5]. The final aim is to get 3D information for the initial packing from 2D statistical properties of the random cut to be able to do the same in the case of *actual* assemblies. Of course, binary systems may behave very differently from monodisperse systems, and polydisperse systems often interpolate between these two extreme situations. Other parameters enter the discussion: The size

*Electronic address: luc.oger@univ-rennes1.fr
†Electronic address: jean-paul.troadec@univ-rennes1.fr

 

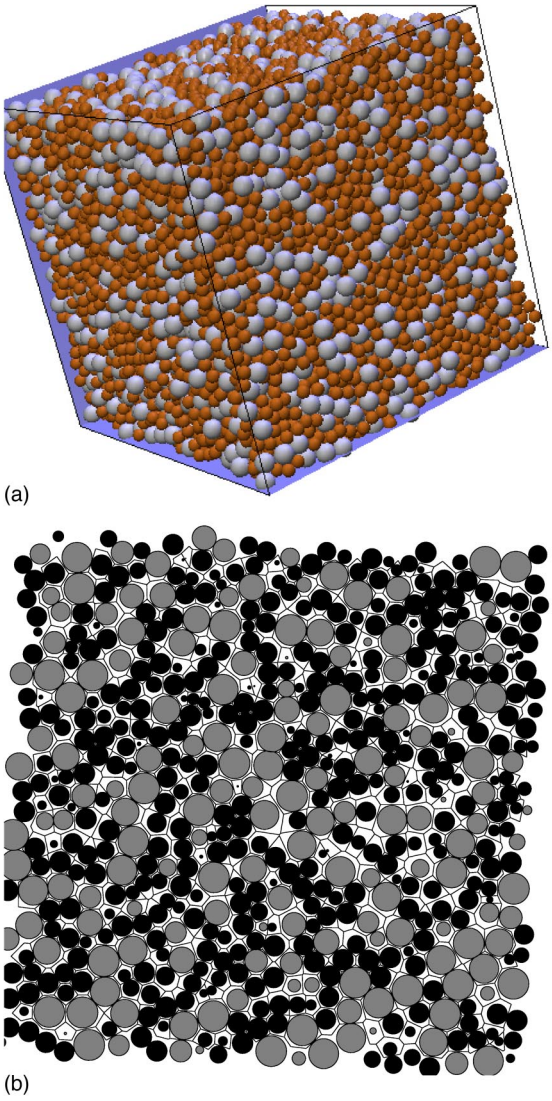


FIG. 1. (a) 3D binary mixture of spheres with 80% of small spheres and a size ratio equal to 1.5. (b) 2D cut of this packing with its radical tesellation, the gray disks correspond to the cuts of the large spheres.

ratio and the numerical fraction of each species. In Sec. II, we recall general stereological relations and their application to the special cases of convex polyhedra fillings and of spheres assemblies. In Sec. III, we describe briefly the building process for our binary packings of spheres and for the related Laguerre cell assemblies. In Secs. IV and V, we give numerical results for the 2D random cuts and check the stereological relations coined in Sec. II. In the last part of Sec. V and in the conclusion, we discuss the method for going upward from 2D to 3D statistics in actual situations.

## II. STEREOLOGICAL RELATIONS

### A. Generalities

The probability for a 3D object $X$ embedded in a vessel $V$ (a cube in our samples) to be sectioned when $V$ is sectioned is [1]

$$H_X/H_V, \tag{1}$$

where $H_X$ and $H_V$ denote the tangent diameter (or orthogonal projection length) of the object and of the vessel relatively to the direction of the sectioning plane. When several sections are performed with random distinct orientations, $H_X$ (resp. $H_V$) is the average projection length. For instance, if the vessel $V$ is a cube with edge length $L$, $H_V=L$ when the cuts are done parallely to one of the sides of the cube and $H_V=3L/2$ when all orientations are equally allowed. If the object $X$ is a sphere of radius $R$, $H_X=2R$. For a polyhedron, $H_X$ reads [1,7]

$$H_X = \frac{1}{2\pi}\sum l_i(\pi-\theta_i)/2, \tag{2}$$

where the sum runs on all edges of the polyhedron, $l_i$ is the length of the $i$th edge, and $\theta_i$ is the inner angle of the dihedron with edge $i$; in the case of a regular polyhedron with $f$ faces, $n$ edges of length $l$ per face and occurence $\lambda$ at each vertex, it simplifies to

$$H_X = \frac{nfl}{8\pi}\cos^{-1}[\cos(\pi/\lambda)/\sin(2\pi/n)], \tag{3}$$

which in the case of tessellations ($\lambda=3$ and $n=n(f)=6-12/f$) reduces further to [1]

$$H_X = \frac{3(f-2)l}{4\pi}\cos^{-1}[1/2\ \sin(2\pi/n)]. \tag{4}$$

For a planar polygon, expression (2) becomes

$$H_X = P/4, \tag{5}$$

where $P$ is the perimeter of the polygon.

Stereological conservation laws exist [1], when going from 3D to 2D cuts, linking the 3D objects in a volume $V$ to their 2D sections on a surface $A$ which may be rewritten as:

(1) Conservation of the packing fraction: The occupied volume per unit volume $V_V$ (or packing fraction $\varphi$) is equal to the occupied area per unit area $A_A$ in the section ($V_V=A_A$ in classical notations),

(2) Conservation of the surface per unit volume $A_V$; more precisely $\pi A_V=4P_A$, where $P_A$ is the perimeter per unit area in the section, and

(3) Conservation of the length per unit volume or $P_V=2Q_A$, where $Q_A$ is the number of traces in the section of the lines with length $P_V$ per unit volume.

### B. Case of assemblies of spheres

We start with a binary mixture of $N$ spheres in a vessel of volume $V_{\text{total}}$ with radii $R_i$, $i=1,2$ ($R_1<R_2$), in numerical proportions $n_i$ ($n_1+n_2=1$). The packing fraction $\varphi$ is the fraction of occupied volume

$$\varphi = \frac{4\pi N}{3}[n_1R_1^3+n_2R_2^3]/V_{\text{total}}, \tag{6}$$

The sections are disordered polydisperse disk assemblies. The number $N_i^*$ of disks issued from spheres of species $i$ in a

section is $N_i^*=Nn_i\,2R_i/H_V$ where $H_V$ is mean tangent diameter of the vessel and $2R_i$ is the tangent diameter of the spheres of type $i$. The total number of disks in the section is $N_1^*+N_2^*=N(n_1\,2R_1+n_2\,2R_2)/H_V$ and the disks issued from spheres of species $i$ are in proportions $n_i^*$

$$n_i^* = n_iR_i/(n_1R_1 + n_2R_2), \tag{7}$$

i.e., the proportion in the cuts *does not* depend on the packing fraction. The conservation laws are contained in the density distribution $P^*(r)$ of sectional disk radii:

$$\begin{cases} P^*(r) = \dfrac{n_1^* r}{R_1\sqrt{R_1^2 - r^2}} + \dfrac{n_2^* r}{R_2\sqrt{R_2^2 - r^2}}, & 0 < r < R_1 \\ P^*(r) = \dfrac{n_2^* r}{R_2\sqrt{R_2^2 - r^2}}, & R_1 < r < R_2. \end{cases} \tag{8}$$

Relation (8) is a simple generalization of the one [1] relative to a monodisperse packing. Alternatively, the fraction $N^*(r)$ of disks with radius less than $r$ is

$$\begin{cases} N^*(r) = 1 - n_1^*\sqrt{R_1^2 - r^2}/R_1 - n_2^*\sqrt{R_2^2 - r^2}/R_2, & 0 < r < R_1 \\ N^*(r) = 1 - n_2^*\sqrt{R_2^2 - r^2}/R_2, & R_1 < r < R_2. \end{cases} \tag{9}$$

Note that repartition function $N^*(r)$ has a cusp at $r=R_1$, with an infinite slope on the left side, and a finite (positive) slope on the right side

$$n_2^*\frac{R_1}{R_2}\frac{1}{\sqrt{R_2^2 - R_1^2}}, \tag{10}$$

which may be large if $n_2^*$ (or $n_2$) is large and/or the size ratio close to 1.

The conservation relations (packing fraction and surface per unit volume), which are more general, may be directly checked by using distribution $P^*(r)$. Of course, these formulas are easily generalized to polydisperse systems and may be also extended to packings of spheres with a continuous radius distribution. Relations (7) and (8) are tested in Sec. IV.

### C. Case of polyhedric tessellations

We consider the case of two-species mixtures of convex polyhedric cells filling space, in numerical proportion $n_i$ $(n_1+n_2=1)$, like the one resulting of the tessellation of a binary mixture of spheres. We restrict to the case where an edge is common to three cells and a vertex to four cells which is the generic case in tessellations [8]. The conservation laws may be rewritten differently and more precise relations exist. The sections are convex polygons filling the plane. For the 3D tessellation, the main information arises from the distribution of neighboring cells. We shall use the classical notations for the partial and total coordination numbers $f_i, \langle f\rangle (\langle f\rangle = \Sigma n_i f_i)$, the fraction $t_{ij}$ of faces common to a $i-$cell and a $j-$cell, the average number $m_i(f)$ (resp. $m(f)$) of faces of the cells neighbor of a $i-$cell (resp. undifferentiated cell) with $f$ faces, and average metric quantities, such as the average cell volume, area, and perimeter per species $V_i, A_i, P_i$, and globally $\langle V\rangle = \Sigma n_i V_i$ and similarly for $\langle A\rangle$ and $\langle P\rangle$. We need also the average value of the perimeter $P_{ij}$ of a face $(ij)$.

The 2D cut of the 3D tessellation is a tessellation of the plane by convex polygons of 2 species. With obvious notations, the corresponding 2D quantities are:

(1) Numerical fraction $\tilde{n}_i$ of cells generated by a 3D $i$-cell,

(2) Coordination number, i.e., average number of neighboring polygons, $\tilde{z}_i$, with $\Sigma\tilde{n}_i\tilde{z}_i=6$ (Euler's identity),

(3) Fraction of neighbors $(ij)$, say $\tilde{t}_{ij}$,

(4) Average number $\tilde{m}_i(n)$ (resp. $\tilde{m}(n)$) of edges of the cells neighbor of a 2D $i-$cell (resp. undifferentiated cell) with $n$ edges, and

(5) metric average quantities, $\tilde{a}_i$, $\tilde{p}_i$ for the average area and perimeter of cells of each species, and $\langle\tilde{a}\rangle$, $\langle\tilde{p}\rangle$ for all cells,…

From the conservation laws (Sec. II A), we derive some relations for binary mixtures:

(1) The number of section polygons $\tilde{N}_i$ of species $i$ is $\tilde{N}_i = N\,n_iH_i/H_V$, where $N$ is the number of polyedra in the vessel with mean tangent diameter $H_V$ and $H_i$ is the average tangent diameter of 3D $i$–cells. The total number of polygons in the section is $\tilde{N}=N(n_1H_1+n_2H_2)/H_V$ and the numerical proportion of polygons of species $i$ in the cut is

$$\tilde{n}_i = n_iH_i\Big/\sum n_iH_i. \tag{11}$$

(2) For each species,

$$\begin{aligned} V_i &= H_i\tilde{a}_i, \\ \pi A_i &= 4H_i\tilde{p}_i, \\ P_i &= 2\tilde{z}_iH_i, \end{aligned} \tag{12}$$

and for the average volume, area, and perimeter

$$\begin{aligned} \langle V\rangle &= \langle\tilde{a}\rangle(n_1H_1 + n_2H_2), \\ \pi\langle A\rangle &= 4\langle\tilde{p}\rangle(n_1H_1 + n_2H_2), \\ \langle P\rangle &= 12(n_1H_1 + n_2H_2). \end{aligned} \tag{13}$$

The last relation is a simple check of the Euler's identity $\tilde{n}_1\tilde{z}_1+\tilde{n}_2\tilde{z}_2=6$ for the 2D mosaics.

(3) Further information on the correlations between neighbors exist. Let $P_{ij}$ denote the average perimeter of a common face $(ij)$ between two cells of species $i$ and $j$. If it is sectioned, it yields a common edge to two 2D section cells and the number of faces $(ij)$ to be sectioned is

$$Ft_{ij}H_{ij}/H_V = Ft_{ij}\frac{P_{ij}}{4H_V} = \tilde{E}\tilde{t}_{ij}, \tag{14}$$

where $F=N\langle f\rangle/2$ is the total number of faces, $\langle f\rangle$ the average number of neighbours of a cell, $H_{ij}=P_{ij}/4$ the tangent diameter for the face $(ij)$ [see Eq. (5)] and $\tilde{E}=3\tilde{N}$ the number of edges in the section. Whence,

$$\tilde{t}_{ij} = t_{ij}P_{ij} \Big/ \sum t_{ij}P_{ij}, \tag{15}$$

or

$$\tilde{t}_{ij} = \langle f \rangle \frac{t_{ij}P_{ij}}{24(n_1H_1 + n_2H_2)}, \tag{16}$$

and

$$\langle f \rangle = 24(n_1H_1 + n_2H_2) \Big/ \sum t_{ij}P_{ij}. \tag{17}$$

These formulas are easily extended to polydisperse assemblies of polyhedra. Relations (11)–(13) and (15) are tested in subsection V C.

## III. NUMERICAL METHODS AND PACKINGS

We first build our binary assembly of spheres, then the related 3D-Laguerre (radical) tessellation and finally perform a random planar cut of the tessellation.

### A. Sphere assembly

We start with two sizes of spheres, with radii $R_i$, $i=1,2$ and $R_1<R_2$, in numerical proportions $n_i$, $n_1+n_2=1$. Except for specific purposes, we shall consider spheres with size ratio $k=R_2/R_1=1.5$. The numerical fraction $n_1$ of small spheres runs from 0.10 to 0.95. We build disordered packings of 16 000 spheres using several types of binary hard core algorithms: Random sequential adsorption (RSA) [9], Powell algorithm [10] (grains are placed successively under gravity), collective algorithms (e.g., event-driven, Jodrey–Tory [11]), which are generalizations of those in the monodisperse case and are detailed in [12]. Let us recall that high packing fractions are realized using Jodrey–Tory algorithm: For the size ratios we have used, the maximal packing fraction $\varphi_m$ slightly depends on $n_1$ but remains close to the maximum value for disordered monodisperse sphere packings, $\varphi_m \sim 0.64$. The Powell algorithm generates a looser packing ($\varphi \sim 0.58-0.60$) and RSA yields dilute assemblies (from 0 to 0.40 at most).

### B. Three-dimensional tessellation

In the case of equal spheres, two grains are said to be neighbors if their Voronoi cell have a common face and a hierarchy in neighbors may be easily generated. The study of the grain assembly is thus complemented with that of the Voronoi tessellation, i.e., of a space filling foam made of convex polyhedral cells, each cell containing one grain and one only [8]. For binary—or more generally polydisperse—systems, a correct generalization of the Voronoi tessellation is the Laguerre (or radical) tessellation [4] where the bisecting plane is replaced by the radical plane with the same topological properties, same occurrence numbers, and one cell containing one sphere and only one. We have now a two-fold froth with two kinds of grains herein.

Note that the 3D Voronoi or radical tessellations are not the most general froth because of the steric constraint. In the monodisperse case, the cells are more regular than those generated for instance by a random Voronoi Poisson process [8,13] and their regularity increases with the packing fraction. It is not so simple in binary cases as the cells are already very differentiated at medium size ratio ($k=1.5$); the "large" cells are probably more regular than the "small" ones.

TABLE I. Fraction of empty cells with $n$ sides for both species ($k=2$, $n_1=0.5$).

| $n$ | Species 1 | Species 2 |
|---|---|---|
| 3 | 1 | 1 |
| 4 | 0.613 | 0.593 |
| 5 | 0.207 | 0.239 |
| 6 | 0.044 | 0.045 |
| 7 | 0.005 | 0.007 |
| 8 | 0.000 | 0.001 |

### C. Random cuts

Once the tessellation is built, we perform a series of at least 40 random sections through each packing, so that the statistical study of the 2D sections is carried out on about 25–30 000 polygonal cells.

Note that some cells are empty as the plane may cut the cell but *not* the sphere. In the samples of this paper (compact assemblies), approximately 75% of the 2D cells are occupied, with more success for the large ones (species 2) as the 3D cells are more regular and thus their faces are closer to the inner sphere. This phenomenon is more accentuated when $k=2$. From Eq. (1), it is easy to check that the fraction of occupied cells of species $i$ is $2R_i/H_i$ and that the fraction of full cells globally is $2(n_1R_1+n_2R_2)/(n_1H_1+n_2H_2)$.

In Table I is plotted the fraction of cells with $n$ sides which are empty for both species. As expected, empty cells have a small number of sides ($n \leqslant 8$); all three cells are empty and nearly two-thirds of the $n=4$ cells. The proportion of empty cells for each $n$ is nearly the same for the two species.

## IV. ASSEMBLIES OF SPHERES

We checked Eqs. (7) and (9) at maximal packing fraction ($\varphi_m \sim 0.64$) and any numerical fraction $n_1$ ($n_1$ running from

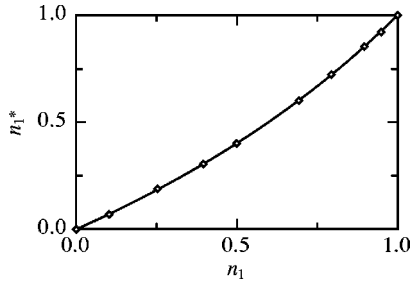


FIG. 2. Plot of $n_1^*$ vs the 3D numerical fraction of small grains $n_1$ for a size ratio $k=1.5$ at maximum packing fraction $\varphi \sim 0.64$; $\diamond$: Numerical values; the theoretical expression is given by the continuous line.

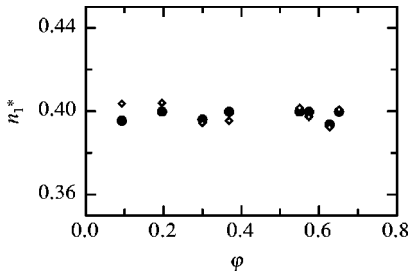


FIG. 3. Plot of $n_1^*$ versus the packing fraction $\varphi$ when $n_1=0.5$ and size ratio is $k=1.5$. $\diamond$: Numerical values, •: Theoretical values. The theoretical values are not all the same because the different building algorithms do not give exactly the same composition and radius ratio.

0.10 to 0.95), then at fixed fraction ($n_1=n_2=0.5$) and increasing packing fraction $\varphi$.

In numerical assemblies, everything is known, i.e., the size ratio $k$, the numerical fraction of small spheres $n_1$ are perfectly determined. Then, the resulting 2D numerical fractions $n_i^*$ and repartition function $N^*(r)$ are easily compared to the theoretical expressions Eqs. (7) and (9). For example, we give in Fig. 2 the variations of $n_1^*$ with $n_1$ for $k=1.5$ at $\varphi \sim 0.64$ and in Fig. 3 $n_1^*$ versus $\varphi$ for $n_1=0.5$ and $k=1.5$. The agreement is very good. In particular, as expected, $n_1^*$ does not depend on the packing fraction.

It is much more interesting to consider that we have an actual sample and that the information only arises from the cuts which is the actual situation. We can determine experimentally the 2D repartition function $N^*(r)$. The presence of a unique cusp at some value of $r$ is characteristic of a binary system. We can then try to fit $N^*(r)$ by the function given by Eq. (9). This has been done using the Levenberg–Marquardt algorithm with parameters $n_1$, $R_1$, and $R_2$. As seen in Fig. 4, the fit is very good. It is still better with a larger size ratio ($k=2$) as the 2 species are drastically separated. It remains good when the size ratio is smaller, even when $n_1$ is small where the determination is more difficult, as seen in Fig. 5 for $k=1.2$ and $n_1=0.2$.

We can compare the final values of the parameters given by the fit algorithm and the numerical values characterizing the 3D packing. The agreement is very good (Table II).

The same study was performed in the case of an *ordered* binary mixture, when the two species are on two shifted simple cubic lattices. Then, $n_1=n_2=0.5$ and the smallest possible size ratio is $k=(\sqrt{3}+1)/2$. We have chosen again $k=1.5$ and $\varphi=0.64$ (the densest packing fraction is $\varphi=18\pi/81=0.67\,873\ldots$). Relations (6) and (10) still hold. The same would probably be true for a segregated packing (large and small grains completely separated); this means that so far it is impossible to get information relative to the positional correlations in the packing with only these general quantities and that a finer analysis is needed. We shall go back to this point in the discussion.

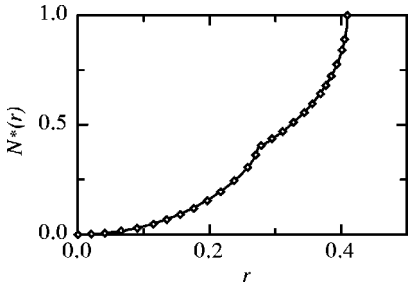


FIG. 4. Plot of $N^*(r)$ for a size ratio $k=1.5$ and $n_1=0.25, \varphi=0.64$; numerical values ($\diamond$) are fitted by the theoretical expression.

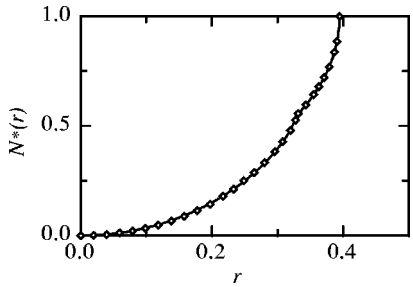


FIG. 5. Fit of the experimental values of $N^*(r)$ to the theoretical expression in a "bad" case: Small size ratio $k=1.2$ and small $n_1=0.20$.

In an experimental study, it would probably be difficult to have a statistics as good as in the numerical case. The samples may be small and only a reduced number of cuts is possible. It is then interesting to study size effects with conditions close to the ones used experimentally in order to have an idea of the reliabiliy of the results of a real experiment. We have then built numerically a large packing of 16 000 spheres with $n_1=0.5$, $k=1.5$, and $\varphi=0.64$. Inside the packing we have made smaller cubic samples of different sizes (10, 12, 16 and 20) measured as the cubic root of the number of spheres in the samples. Four (nonoverlapping) samples were considered for sizes 10 and 12, two for size 16 and one for size 20. Through each sample, we have made 40 cuts parallel to its sides, choosing randomly one of the three directions and the position of each cut. Table III gives the statistical results we have obtained. The largest difference between the mean value of the parameters of the fit and the numerical value is less than 1% for $R_1$ and $R_2$ and about 2% for $n_1$. As expected, the mean square deviation $\sigma$ decreases when the size of the sample increases. For all sizes, it is small for $R_1$ ($\sim$3% at size 10) and even smaller for $R_2$: the radii are obtained with a good precision from a few cuts. It remains large for $n_1$ and a large number of cuts is necessary to determine $n_1$ precisely.

TABLE II. Comparison of the parameters given by the fit with the numerical values of the 3D packing.

| | $k=1.5$ | | $k=1.2$ | |
|---|---|---|---|---|
| | Fit | Num. | Fit | Num. |
| $n_1$ | 0.2550 | 0.2533 | 0.2088 | 0.2048 |
| $R_1$ | 0.2730 | 0.2730 | 0.3264 | 0.3287 |
| $R_2$ | 0.4095 | 0.4095 | 0.3944 | 0.3944 |

TABLE III. Size effects for cuts parallel to the sides of the cubic sample. Numerical values: $R_{1num}=0.2441$, $R_{2num}=0.3670$, and $n_{1num}=0.4996$.

| Sample size → | 10 | 12 | 16 | 20 |
|---|---|---|---|---|
| $R_{1fit}$ | 0.2451 | 0.2441 | 0.2439 | 0.2442 |
| $R_{2fit}$ | 0.3650 | 0.3653 | 0.3661 | 0.3663 |
| $n_{1fit}$ | 0.4893 | 0.5101 | 0.4968 | 0.4951 |
| $\sigma_{R_1}$ | 0.0076 | 0.0042 | 0.0036 | 0.0002 |
| $\sigma_{R_2}$ | 0.0029 | 0.0022 | 0.0015 | 0.0006 |
| $\sigma_{n_1}$ | 0.093 | 0.086 | 0.053 | 0.040 |

## V. RESULTS FOR THE CUT OF THE TESSELLATION

As explained in the preceding section, in numerical ensembles everything is known. So, all 3D and 2D quantities may be reached. We first recall briefly the 3D behavior of the Laguerre tessellation (see [12]), then give the results for the 2D cuts and check the stereological relations of Sec. II.

Except when explicitly noticed, the 3D and 2D tessellations have been generated from sphere assemblies for a size ratio $k=1.5$ and maximal packing fraction ($\varphi_m \sim 0.64$).

### A. Analysis of the three-dimensional cell assembly

Such an analysis was already performed in [12]. We briefly recall main statistical properties.

(1) For $k=1.5$, the 3D cells of the two species are clearly different and the distribution functions for the fraction $p_i(f)$ of $f$-faced cells of species $i$ and for the metric quantities $V_i$, $A_i$, and $P_i$ are clearly separated, all distributions presenting two separated peaks and a very weak overlap.

(2) Both coordination numbers $f_i$ are increasing functions of $n_1$. At the two limiting situations $n_1=0$ (resp. $n_2=0$), $f_2$ . (resp.$f_1$)$=\langle f\rangle \sim 13.9$

(3) The total number of faces $fm_i(f)$ of the neighbors of a $f$-faced cell of species $i$ is a linear function of $f$ (Aboav's law [14]). It is not true for a global analysis of the packing. This is better put into evidence for a larger size ratio $k=2$ (Fig. 6).

(4) The average volume, area and perimeter $V_i(f)$, $A_i(f)$, and $P_i(f)$ for species $i$ and at given $f$ are not linear functions of $f$, contrary to the monodisperse case where Lewis and Desch laws hold [15,16].

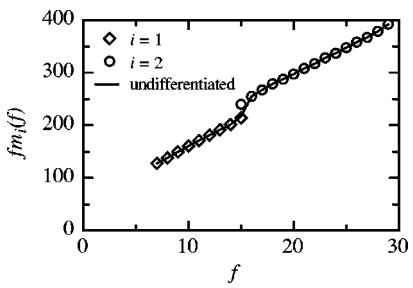


FIG. 6. Aboav's law holds for the two species separately, but not for the global analysis of the packing ($k=2$, $n_1=0.75$).

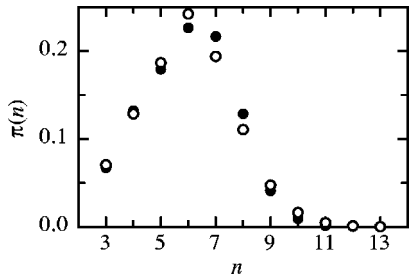


FIG. 7. Distribution $\pi(n)$ of the number of sides of a cell ($k=1.5$, full circles $n_1=0.25$, empty circles $n_1=0.80$).

### B. Analysis of the two-dimensional cell assembly

In the following, we shall consider the 2D mosaics resulting from a planar random section independently of the underlying sphere packing which may just be considered as an intermediate for building a 3D froth. It would not be possible in actual sphere assemblies and we shall go back to this point in the conclusion.

We go now to the corresponding 2D quantities and check similarities and differences with the 3D case.

(1) The proportion $\tilde{n}_1$ of sections related to species 1 is an increasing function of $n_1$ like $n_i^*$ and always $n_1^* < \tilde{n}_1$.

(2) The total distribution function $\pi(n)$ for the number $n$ of sides of a cell has only one peak (Fig. 7); the same is true for the distribution of the area of the cells.

(3) The partial coordination numbers $\tilde{z}_i$ are increasing functions of $n_1$ (Fig. 8). They satisfy the Euler's relation $\tilde{n}_1\tilde{z}_1+\tilde{n}_2\tilde{z}_2=6$. At the limit $n_1=0$, $\tilde{z}_2=\tilde{z}=6$ and conversely.

(4) The fractions $\tilde{t}_{ij}$ of common edges $(ij)$ have been plotted on Fig. 9 as a function of $n_1$. The behavior is qualitatively the same as for the $t_{ij}$ in the 3D tessellation.

(5) Aboav's empiric law *for each species* holds and also for the global analysis of the packing (Fig. 10):

$$n\tilde{m}_i(n) = (6-\lambda_i)n + \gamma_i. \tag{18}$$

(6) We have measured all metric quantities such as the area and perimeter of each cell, the average area $\tilde{a}_i$ and perimeter $\tilde{p}_i$ per species and we have analyzed their distribution function. Contrary to the 3D case, the two peaks are not separated. As to the areas $\tilde{a}_i$ (resp. perimeter $\tilde{p}_i$) we have checked their dependence on the number of sides $n$ of the

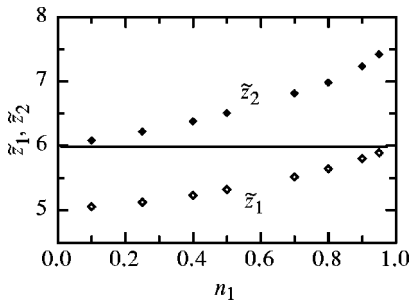


FIG. 8. Variation of the partial coordination numbers $\tilde{z}_i$ with $n_1$ ($k=1.5$).

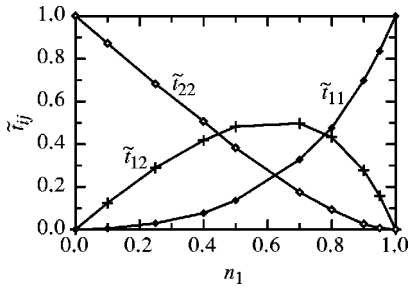


FIG. 9. Variation of the $\tilde{t}_{ij}$ with $n_1$ ($k=1.5$).

section cells…Neither Desh [16] nor Lewis [15] laws hold (Fig. 11).

### C. Check of the stereological relations

We have first checked on our numerical assemblies the stereological relations (11)–(15) derived in Sec. II C. The agreement is pretty good even when $n_1$ or $n_2$ are small and the statistics poor in one species. As an example, in Table IV, the theoretical and numerical values of the $\tilde{t}_{ij}$ are compared.

However, going backward from 2D to 3D with the only 2D information is not straightforward. First, pure individual average quantities require the knowledge of the tangent diameter $H_i$ of the 3D $i$-cells: from the number $N$ of 3D cells and the average number $\tilde{N}$ of cells in a section, it is easy to know the global average tangent diameter $n_1H_1+n_2H_2$ and from $\tilde{n}_i$ to get back the average tangent diameter of each species, provided $n_i$ is known. If not, the problem is harder and only $n_iH_i$, then 3D quantities such as $n_iV_i$, $n_iA_i$, $n_iP_i$…can be reached. Note that, in the case of a binary sphere packing, it is possible to get $n_i$ and $R_i$ separately and then all 3D individual average quantities. The 3D coordination numbers $\langle f\rangle$, $f_i$ require the knowledge of the average perimeters $\langle P\rangle$, $\langle P_i\rangle$ of the 3D cells which may be derived from the conservation laws (12). However, correlations are harder to get, as the $t_{ij}$ require the knowledge of the individual perimeters $P_{ij}$.

### D. Open problems

Let us go now to an actual situation and more precisely let us consider *an actual packing* modeled by (possibly polydisperse) spheres.

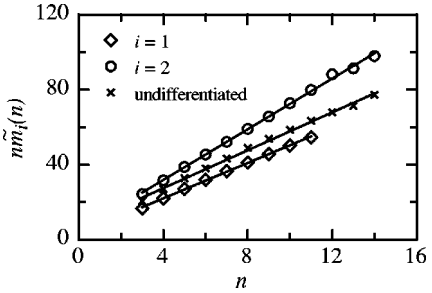


FIG. 10. Aboav's law holds for the two species and for the undifferentiated case ($k=2$, $n_1=0.75$).

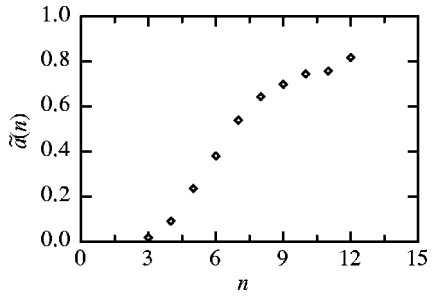


FIG. 11. Variation of the area $\tilde{a}(n)$ of the cells with $n$ ($R_1=0.296$, $k=1.5$, $n_1=0.5$).

In that case, the 3D tessellation is not known, the only information available is the set of planar disks. As seen in Sec. IV, not much may be done directly with the set of sectional disks. However, another partition of the plane may be performed, from the Laguerre tessellation in the section (and not from the cut of the tessellation) as was already done for 2D binary and polydisperse assemblies of disks [17]: there are less cells (about 25% less in our compact assemblies) but larger cells. Their edges often coincide with the edges of the cut of the tessellation as, when the section disk exists, the radical axis is the trace of the radical plane in the section; on the other hand, non-neighboring spheres may have neighboring disks in the section and this will be the main problem when going back from 2D to 3D.

We denote by an asterisk the quantities related to the tessellation of the section. Qualitatively, the two tessellations do not look very different at first sight. For a size ratio $k=1.5$, topological quantities $z_i^*$ and $\tilde{z}_i$ on one hand and $t_{ij}^*$ and $\tilde{t}_{ij}$ on the other are rather close; numerical differences begin to be noticeable when $k\sim 2$. As for the cut of the tessellation Aboav's law holds for each species separately (but not globally); Lewis and Desch empirical laws do not.

However, in spite of some common features, the two tessellations are not simply numerically related and it is not possible to derive properties of the cut of the tessellation (unknown on experimental samples) from the properties of the tessellation of the cut. Moreover, the main differences concern the distribution functions which are narrower in the tessellation of the cut as can be seen, e.g., on the dispersion

TABLE IV. Comparison of the stereological formulation values with the numerical values for the correlation functions $\tilde{t}_{ij}$.

| | $\tilde{t}_{11}$ | | $\tilde{t}_{12}$ | | $\tilde{t}_{22}$ | |
|---|---|---|---|---|---|---|
| $n_1$ | theory | stereo. | theory | stereo. | theory | stereo. |
| 0.10 | 0.044 | 0.044 | 0.1268 | 0.1256 | 0.8688 | 0.8700 |
| 0.25 | 0.0293 | 0.0291 | 0.2938 | 0.2886 | 0.6769 | 0.6823 |
| 0.40 | 0.0785 | 0.0777 | 0.4224 | 0.4197 | 0.4991 | 0.5026 |
| 0.50 | 0.1396 | 0.1396 | 0.4844 | 0.4844 | 0.3760 | 0.3760 |
| 0.70 | 0.3292 | 0.3285 | 0.4981 | 0.4950 | 0.1727 | 0.1765 |
| 0.80 | 0.4830 | 0.4777 | 0.4295 | 0.4299 | 0.0875 | 0.0923 |
| 0.90 | 0.6978 | 0.6976 | 0.2785 | 0.2781 | 0.0238 | 0.0243 |
| 0.95 | 0.8390 | 0.8395 | 0.1548 | 0.1543 | 0.062 | 0.0063 |

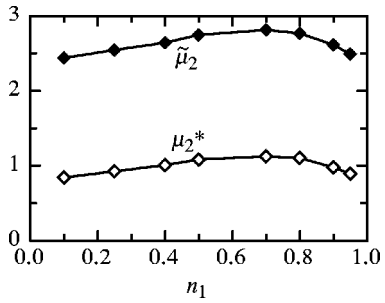


FIG. 12. Dispersion of the number of sides of the cells in the cut of the tessellation ($\tilde{\mu}_2$) and in the tessellation of the cut ($\mu_2^*$) ($k=1.5$).

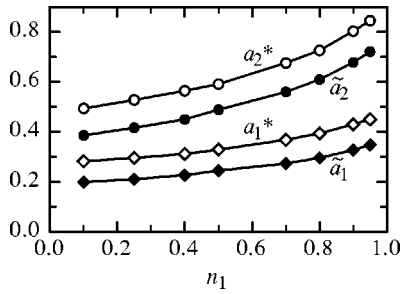


FIG. 13. Average areas of the two types of cells in the cut of the tessellation ($\tilde{a}_1$ and $\tilde{a}_2$) and in the tessellation of the cut ($a_1^*$ and $a_2^*$) ($k=1.5$).

of the number of sides of the cells in both cases ($\mu_2^*$ and $\tilde{\mu}_2$) (Fig. 12). As to metric quantities, by construction, areas and perimeters are greater in the tessellation of the cut, [$a_1^*$ and $a_2^*$ are, respectively, 1.4 and 1.25 larger than $\tilde{a}_1$ and $\tilde{a}_2$ (Fig. 13)] but overall, the distributions again are more peaked: The dispersion of partial areas $a_i^*$ is smaller nearly by a factor 2 for $k=1.5$ in the tessellation of the cut.

## VI. CONCLUSION

We have studied binary mixtures of spheres together with the froth generated by their related Laguerre-Voronoi tessellation. The cut of the tessellation is in turn a disordered 2D tessellation (mosaic) made of two species of convex cells. We have derived the main stereological relations between the 3D tessellation and its 2D cut and checked their accuracy on numerical assemblies. The agreement is very good.

However, in actual samples, going from 2D to 3D information as to the shape or relative arrangement of the grains is not so easy. Already for disordered sphere assemblies, only the numerical fraction and radii of each species may be easily reached. For convex polyhedral assemblies filling space, getting individual average quantities implies the knowledge of the tangent diameter $H_i$, which is possible, but the determination of correlated quantities depends on the knowledge of the 3D perimeters $P_{ij}$ of the faces of the cells which is a more difficult problem.

In the extension to the studies of granular materials, a possibility could be the construction of the tessellation in the cut, which can be performed on actual samples, although the correspondence with the cut of the tessellation is only partial. One may hope then to reconstruct the 3D tessellation and thus study the actual 3D geometrical organization. We are presently beginning this study.

[1] E. R. Weibel, *Stereological Methods* (Academic, New York, 1980) Vol. 2.
[2] J. V. Sanders, Philos. Mag. A **42**, 705 (1980).
[3] O. Sonneville-Aubrun, V. Bergeron, T. Gulik-Krzywicki, B. Jönsson, H. Wennerström, P. Linder and B. Cabane, Langmuir **16**, 1566 (2000).
[4] B. Gellatly and J. Finney, J. Non-Cryst. Solids **50**, 313 (1982).
[5] L. Oger, P. Richard, J. P. Troadec, and A. Gervois, Eur. Phys. J. B **14**, 403 (2000).
[6] W. M. Visscher and M. Bolsterli, Nature (London) **239**, 504 (1972).
[7] K. Voss, J. Microsc. **128**, 111 (1982).
[8] A. Okabe, B. Boots, and K. Sugihara, *Spatial Tessellations Concepts and Applications of Voronoi Diagrams* (Wiley, New York, 1992).
[9] E. L. Hinrichsen, J. Feder, and T. Jossang, J. Stat. Phys. **44**, 793 (1986).
[10] M. Powell, Powder Technol. **25**, 45 (1980).
[11] W. S. Jodrey and E.Tory, Powder Technol. **30**, 111 (1981).
[12] P. Richard, L. Oger, J. P. Troadec, and A. Gervois, Physica A **259**, 205 (1998).
[13] J. L. Meijering, Philips Res. Rep. **8**, 270 (1953).
[14] D. A. Aboav, Metallography **3**, 383 (1970).
[15] F. T. Lewis, Anat. Rec. **38**, 341 (1928).
[16] H. Desch, J. Inst. Met. **22**, 241 (1919).
[17] C. Annic, J. P. Troadec, A. Gervois, J. Lemaitre, M. Ammi, and L. Oger, J. Phys. I **4**, 115 (1994).